Indian Journal of Chemistry
Vol. 54A, November 2015, pp. 1394-1401

Effect of activators and calcination on luminescence properties of åkermanite type phosphors

Erkul Karacaoglu[a,*] & Bekir Karasu[b]

[a]Karamanoglu Mehmetbey University, Engineering Faculty, Department of Materials Science and Engineering, Karaman, Turkiye
Email: ekaracaoglu@kmu.edu.tr

[b]Anadolu University, Engineering Faculty, Department of Materials Science and Engineering, Eskisehir, Turkiye

Received 1 October 2015; revised and accepted 27 October 2015

Ákermanite type $Ca_2MgSi_2O_7$ phosphors activated with different types of rare earths have been synthesized through a solid state reaction method under weak reducing atmosphere and/or open atmosphere. The phase properties of the samples are characterized by X-ray diffraction and the effects of rare earth ions ($Eu^{2+/3+}$, Dy^{3+}, Ce^{3+}, Sm^{3+} and $Pr^{3+/4+}$) and calcination atmosphere on the luminescence properties of the $Ca_2MgSi_2O_7$ host are investigated by using a photoluminescence spectrometer. The comparative results of SEM and laser particle size analysis reveal that the relatively regular morphology, smaller particle size and narrow size distribution can be achieved for the phosphor synthesized by the solid state reaction method including dry-milling below 170 mesh. In the photoluminescence investigations, all the activator ions show different emissions for $Ca_2MgSi_2O_7$ host lattice. The results show that the luminescence properties of rare earth ions activated $Ca_2MgSi_2O_7$ host are also highly dependent on the calcination conditions.

Keywords: Phosphors, Ákermanite, Solid state reaction, Activators, Calcination, Luminescence, Rare earths

In recent years, as a new generation of long persistent phosphors, the rare earths-activated alkaline earth silicates and aluminates having high chemical stability, water resistance and color variation have been extensively studied due to a growing market demand for their applications in traffic signals, emergency exit routes, decoration, and textile printing, with ceramics, glasses, polymers or metals.

The host compound $Ca_2MgSi_2O_7$ belongs to the $CaO\text{-}MgO\text{-}SiO_2$ ternary system. Four Ca-Mg-Si-O compounds, such as monticellite ($CaO\text{-}MgO\text{-}SiO_2$:$CaMgSiO_4$), diopside ($CaO\text{-}MgO\text{-}2SiO_2$:$CaMgSi_2O_6$), åkermanite ($2CaO\text{-}MgO\text{-}2SiO_2$:$Ca_2MgSi_2O_7$), and merwinite ($3CaO\text{-}MgO\text{-}2SiO_2$:$Ca_3MgSi_2O_8$), exist in this system. The åkermanite type materials are one of the end-members of the melilite family of minerals ($A_2BT_2O_7$, A: Ca/Na, B: Mg/Al/Fe(II), T: B/Al/Si). The $Ca_2MgSi_2O_7$ chosen for the present studies crystallizes in a tetragonal space group $P\bar{4}2_1m$ in which the calcium ions are 8-fold coordinated, while both the Mg^{2+} and Si^{4+} ions are tetrahedrally surrounded by oxygen anions. Since in this structure type two SiO_4^{4-} tetrahedra share a corner, Åkermanite belongs to the family of sorosilicates. The $Ca_2MgSi_2O_7$ is also well known as a host for persistent phosphors, generally activated with several rare earth ions, such as Eu^{2+}, Nd^{3+}, Dy^{3+} or Mn^{2+}. When Eu^{2+} and Mn^{2+} are used as dopant ions, the phosphors are potential candidates to be used in LEDs for the generation of white luminescence. In recent years, it has also been studied for biological and medical applications[1]. Eu^{2+} doped $Ca_2MgSi_2O_7$ phosphors are known as efficient phosphors with good stability[2-5]. The optical properties of Eu^{2+} doped $CaMgSi_2O_6$ have been reported by Jung *et al.*[3] Moreover, the luminescence of $M_3MgSi_2O_8$: Eu^{2+} (M = Ca, Ba, Sr) and $BaMg_2Si_2O_7$: Eu^{2+} has also been reported[4]. Furthermore, the long-lasting yellow color emitting phosphor, $Ca_2MgSi_2O_7$: Eu^{2+}, Dy^{3+}, where Dy^{3+} mainly acted as trap center, has been investigated[6]. The phosphorescence behavior of $Ca_2MgSi_2O_7$ phosphors activated with different rare earths are expected to a different and observable when the samples are prepared in different atmosphere, although the origin of such differences is not fully understood, and no detailed studies have been repeated.

Therefore, it was decided to investigate the photoluminescence properties (PL) in $Ca_2MgSi_2O_7$: Eu/Dy/Ce/Sm/Pr synthesized in different atmospheres. With this goal in mind, a series of Eu_2O_3, Dy_2O_3, Ce_2O_3, Sm_2O_3, Pr_6O_{11} separately added

to $Ca_2MgSi_2O_7$ as luminescent center and were prepared in N_2/H_2 and/or air (open) atmospheres, respectively. So, there are both similar results with previous researchs and also novel results of this structure with rare-earths.

Material and Methods

In the present study, the phosphors were synthesized via high temperature solid-state reaction method, also known as ceramic method. Using the base composition of $Ca_2MgSi_2O_7$: ~0.5 mass% REO (Rare Earth Oxides-REO= Eu_2O_3, Ce_2O_3, Pr_6O_{11}, Sm_2O_3, Dy_2O_3), appropriate amounts of the high purity starting reagents, $CaCO_3$ (Merck, Suprapur, 99.95%), $Mg(OH)_2$ (Aldrich, 95%) and SiO_2 (Merck, highly dispersed suitable for use as excipient) and a small amount the fluxing agent, H_3BO_3 (Eti Maden, Turkiye, 99.9%), were thoroughly mixed and ground in a planetary mill (Fritsch/Pulverisette 5) at 250 rpm for 1.5 h in propanol-2 which was added to facilitate the grinding process and to enhance the particle mixing. Subsequently, the mixed slurry forms were dried in an oven at 100 °C for 5 h. Then, the mixed powders were heated in pure alumina crucibles using a tubular furnace (Protherm PTF 16/50/450) at 1100–1400 °C for 1-4 h under weak reducing atmosphere of 90–97% N_2 + 10–3% H_2 gas mixture. In addition, the powders were also heated using a open atmosphere furnace and then cooled down to the room temperature slowly. The synthesized phosphors were ground to powder form and screened to pass 170 mesh sieves prior to the characterization.

Simultaneous differential thermal analysis (DTA) and thermogravimetric (TG) analysis (Seiko Instruments Inc./Exstar TG/DTA 6200) at a heating rate of 10 °C/min from room temperature to 1350 °C were carried out to analyze the decomposition and the oxidation process of the precursor. The particle size analysis was done on a Malvern Instruments Mastersizer Hydro 2000G laser particle size analyzer. The morphology and particle size distribution of the calcined, dry-milled and sieved powders were designated with a Zeiss EVO 50 scanning electron microscope (SEM). A Rigaku Rint 2000 X-ray diffractometer, run at 40 kV and 30 mA (Cu-Kα radiation) in a step-scan mode (2°/2θ), was used to determine phases after calcination. The excitation and emission spectra of the synthesized phosphors were recorded on a fluorometer (Photon Technology International (PTI), QuantaMaster™ 30).

Results and Discussion

Thermal analysis

To examine the thermal stability of $Ca_2MgSi_2O_7$ which is composed of $CaCO_3$ and $Mg(OH)_2$ and SiO_2, DTA/TG analyses were carried out with the raw material mixture between 50 °C and 1350 °C (Fig. 1).

As shown by Fig. 1, the initial weight loss from the former precursor for about 2% from room temperature to 250 °C is due the evaporation of the physically absorbed water from the raw materials mixture. The first major weight loss step is found in the temperature range of 250–440 °C, being due to the transition phase, $Mg(OH)_2 \rightarrow MgO + H_2O$. The first

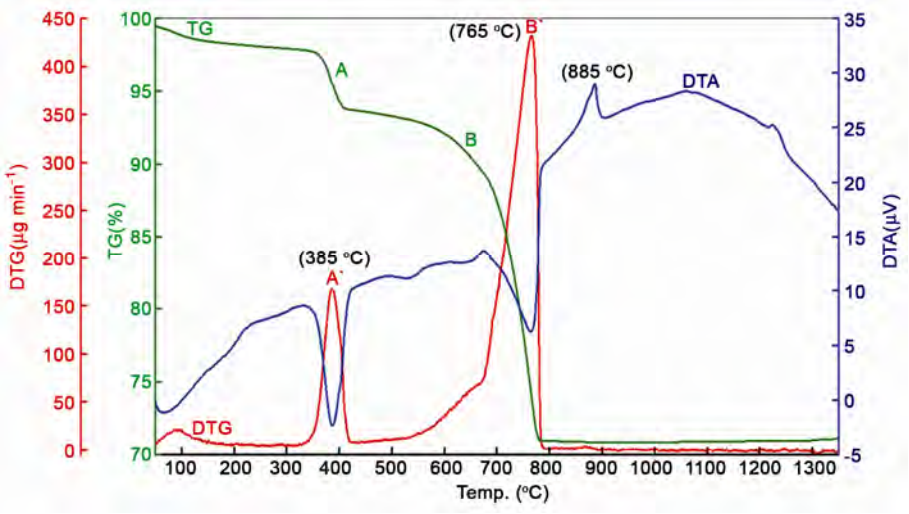

Fig. 1—TG and DTA results of the oxide/carbonate/hydrate mixtures prepared by ceramic method with identical target lattice composition of $Ca_2MgSi_2O_7$:0.006RE.

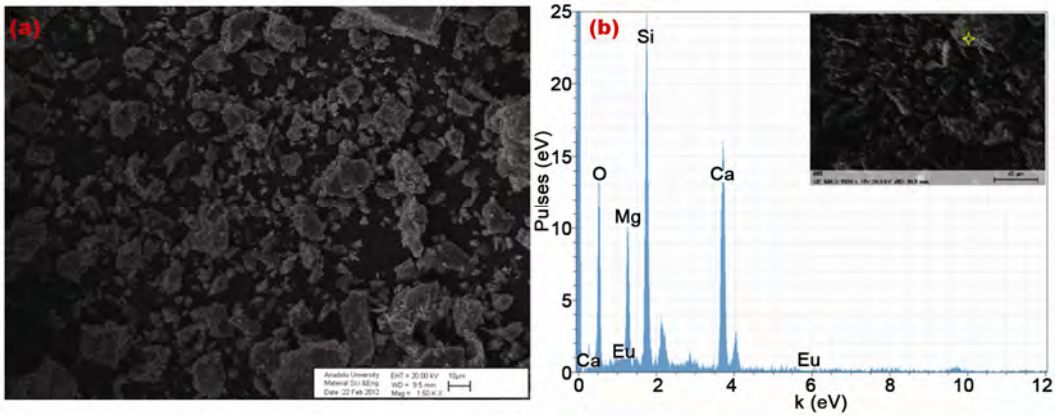

Fig. 2—(a) SEM image and (b) EDX data of Eu-doped $Ca_2MgSi_2O_7$ phosphor ground and sieved under 170 mesh.

sharp drop of weight corresponds to the endothermic peak at 385 °C. The second endothermic peak appearing in the range 430–800 °C corresponds to the decomposition of magnesium hydroxide and regulation of the $Mg(OH)_2$ structure to that of pure MgO, accompanied by the loss of structural water. This rapid mass decrease corresponding to the endothermic effect was indicated in the TG results[6].

The second stage weight loss 510–790 °C is also related to the decomposition of $CaCO_3$ which occurs in a single step in a defined way due to carbon dioxide release, given rise to calcium oxide: $CaCO_3(s) \rightarrow CO_2(g) + CaO(s)$ corresponding to the endothermic peak at 765 °C in its DTA curve[7]. The exothermal peak at 884 °C is believed to be the crystallization temperature for the first formation of $Ca_2MgSi_2O_7$ in the solid state-assisted process; also the precursor continues to crystallize at 1224 °C as indicated by a second clear exothermal peak. The TG curve exhibits a total mass loss of 26.50%, which is almost similar the calculated mass loss (26.48%) attributed to the complete dehydroxylation process of $Mg(OH)_2$ and $CaCO_3$.

Particle size and characterization

After calcination at optimum temperature of 1300 °C, for 2 h to get the dominant $Ca_2MgSi_2O_7$ phase, the samples were dry-ground and sieved under 170 mesh for characterization, e.g. SEM, XRD and PL. The comparative particle size distribution of $Ca_2MgSi_2O_7$ based phosphor samples, into which the rare earths ions were separately doped, were analyzed by laser particle size analysis. The particle size distribution of the $Ca_2MgSi_2O_7$ based phosphor samples was found to be $d(0.1)$: 2.535 mm, $d(0.5)$: 15.390 mm and $d(0.9)$: 63.256 mm.

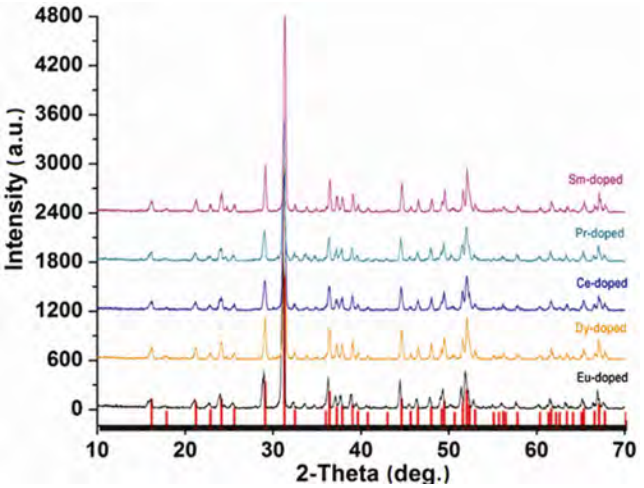

Fig. 3—XRD patterns of $Ca_2MgSi_2O_7$ phosphors activated with different rare earth ions and heated at 1300 °C for 2 h.

SEM and particle size analysis results show that the grains are irregular in shape with a average particle size of ~15 µm. SEM and EDX of Eu-doped $Ca_2MgSi_2O_7$ based phosphor samples are shown in Fig. 2 as representative. For the Dy, Ce, Pr and Sm-doped $Ca_2MgSi_2O_7$ phosphors, see Figs S1-S4 (Supplementary Data). EDX analysis showed that all the $Ca_2MgSi_2O_7$ based phosphors have mainly Ca, Mg and Si and small amounts of the rare earth elements Eu, Dy, Ce, Pr and Sm (Fig. 2(b) and Supplementary Data, Figs S1 - S4 (b)).

X-ray diffraction (XRD) analysis

Figure 3 depicts that the XRD patterns of the samples indicating the major peaks which can be indexed to $Ca_2MgSi_2O_7$ in a tetragonal structure (JCPDS 87-0052).

This single-phase sample is well crystallized at 1300 °C for 2 h. Since no impurity phase was

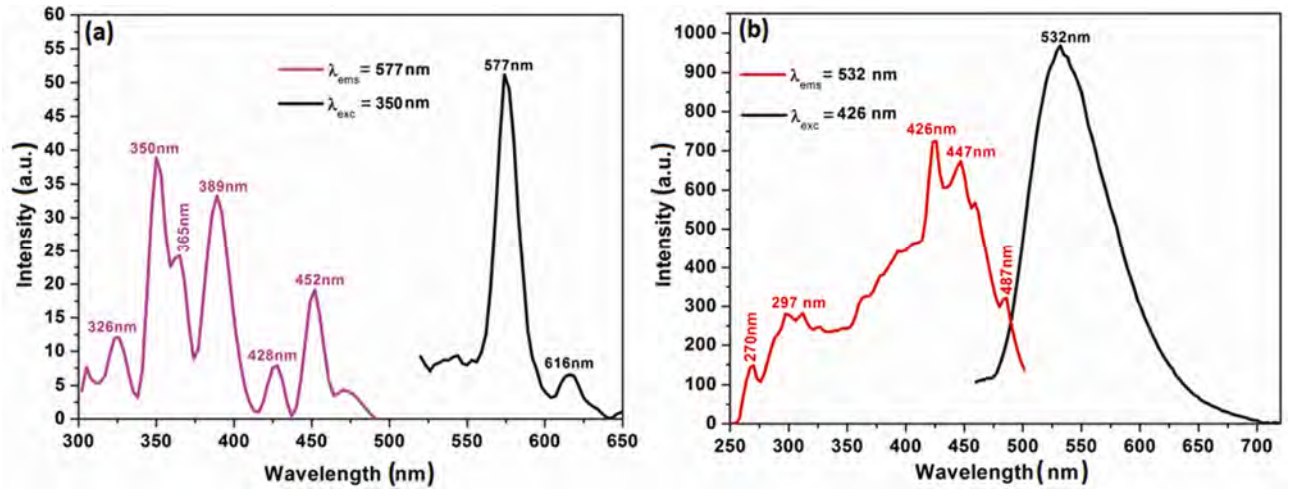

Fig. 4—Excitation and emission spectra of $Ca_2MgSi_2O_7$:0.006Eu^{3+}/Eu^{2+} synthesized in (a) open atmosphere and (b) weak reducing atmosphere.

observed in any of the samples, it clearly implies that the obtained samples are single phase and doping does not cause any significant change in the host structure or lattice distortions.

Photoluminescence properties

The excitation and emission spectra of Eu_2O_3 added $Ca_2MgSi_2O_7$ phosphors, calcined in open atmosphere as well as weak reducing atmosphere are presented in Fig. 4.

Eu_2O_3 added $Ca_2MgSi_2O_7$ phosphor calcined in weak reducing atmosphere has an emission band being at 532 nm in yellowish-green color region (Fig. 4(b)). The relative strong intensity of Eu^{2+} observed in its emission spectrum is due to the $4f^6 5d^1 \rightarrow 4f^7$ transition of the Eu^{2+} ion because of the reducing atmosphere calcination conditions as reported in recent studies[2,3]. Divalent europium ion (Eu^{2+}) is one of a well known activator in phosphors for application in modern lighting, displays, and optical communications fields such as light-emitting diodes (LEDs), long-lasting phosphors (LLPs), fluorescent lamps and plasma display panels (PDPs)[9-12]. According to the structural studies, there is only one eight-coordinated Ca^{2+} site in the tetragonal $Ca_2MgSi_2O_7$ lattice[13]. It was predicted that Eu^{2+} and Mn^{2+} tend to substitute the Ca^{2+} and Mg^{2+} sites, respectively, because the ionic radii of Eu^{2+} (1.25 Å) and Mn^{2+} (0.66 Å) are compatible with those of Ca^{2+} (1.12 Å) and Mg^{2+} (0.57 Å). Also, the Si^{4+} site (0.26 Å) is too small for the Eu^{2+} and Mn^{2+} occupation to take place. When Eu replaces Ca in the $Ca_2MgSi_2O_7$ phosphor, it will occupy two different kinds of lattice sites (Eu1 and Eu2) with coordination numbers of six or eight[14].

In the emission and excitation spectra of Eu^{3+}-doped, or in other words, Eu_2O_3-activated $Ca_2MgSi_2O_7$ calcined in oxidized atmosphere measured at room temperature (Fig. 5(b)), the following emission transitions were observed: $^5D_0 \rightarrow {}^7F_1$ at 577 nm and $^5D_0 \rightarrow {}^7F_2$ at 616 nm (611–620 nm), of which the $^5D_0 \rightarrow {}^7F_1$ transition is stronger. Eu^{3+} ions emit a characteristic red light with several narrow lines due to the $4f \rightarrow 4f$ ($^5D_0 \rightarrow {}^7F_{i\,=\,0,1,2,3,4}$) transitions. The luminescence spectrum of Eu^{3+} ion is slightly influenced by the surrounding ligands of the host material because the transitions of Eu^{3+} involve only a redistribution of electrons within the inner $4f$ sub-shell[14,15]. The excitation spectra of these phosphor samples show that they can be well excited by near UV-light which is exactly as required by ultra-violet chip pumped multi-phosphor converted white LEDs.

Dy^{3+} ions have been often used as co-dopant in long afterglow phosphorescent pigments. When divalent alkaline earth ions, such as Ca^{2+} or Sr^{2+}, are substituted by trivalent Dy^{3+} in the alkaline earth silicates and aluminates, various defects can be induced due to the charge compensation mechanism, among which alkaline earth ion vacancy (VM), is the principal one. VM is considered to be the hole trap, while Dy^{3+} occupying alkaline earth ion sites is a very probable source of electron trap. In the Eu^{2+} activated and the Dy^{3+} co-doped long afterglow phosphors, such as $SrAl_2O_4$: Eu^{2+}, Dy^{3+}, Y^{3+} or $Sr_4Al_{14}O_{25}$: Eu^{2+}, Dy^{3+}, most of the excitation energy will be transferred from the host or the Dy^{3+} to the Eu^{2+}. Thus, only $5d$-$4f$ emissions of Eu^{2+} can be observed[9-12]. However, in the current study it is thought that in Dy^{3+} singly

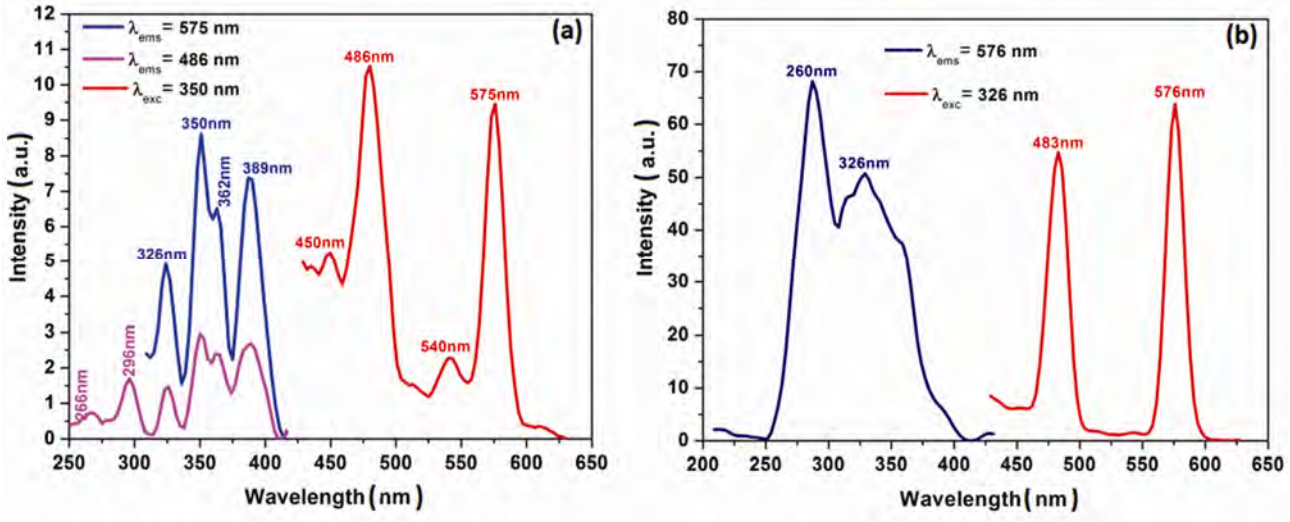

Fig. 5—Excitation and emission spectra of (a) $Ca_2MgSi_2O_7:Dy^{3+}$ and (b) $Ca_2MgSi_2O_7:Dy^{3+}$, Ce^{3+} (right) synthesized in weak reducing atmosphere.

doped hosts, Dy^{3+} may be not only the supplier of traps but also an activator itself, as mentioned previously in the literature[5].

The excitation and the emission spectra of the only Dy^{3+} doped and also Dy^{3+}-doped with Ce^{3+}-co-doped $Ca_2MgSi_2O_7$ samples are given in Fig. 5. Dy^{3+} ions, which show luminescence lines in the 470–500 nm region due to $^4F_{9/2}$-$^6H_{15/2}$ transition and in the 570–600 nm region due to the $^4F_{9/2}$-$^6H_{13/2}$ transition, have attracted much attention because of the white emission in the visible region of electromagnetic spectra. For the Dy^{3+} single-doped $Ca_2MgSi_2O_7:Dy^{3+}$ phosphor (Fig.5(a)), the excitation spectra for the emission at both 575 nm and 486 nm comprise a series of line spectra in the 250–430 nm region with the strongest line at 350 nm and some lines at 266, 296, 326, 362 and 389 nm, which are ascribed to the transitions from the ground state to excited states in the $4f^9$ configuration of Dy^{3+}; however these are not clearly assigned due to the dense and somewhat overlapping levels of 4*f* configuration of Dy^{3+} in the high energy region. The blue emission peaking at 486 and yellow emission peaking at 575 nm were observed and may be assigned to the $^4F_{9/2}$-$^6H_{15/2}$ and $^4F_{9/2}$-$^6H_{13/2}$ transitions of Dy^{3+}, respectively[16].

Both the excitation and the emission spectra of Dy^{3+}-activated and Ce^{3+} co-doped $Ca_2MgSi_2O_7$ samples comprise the characteristic lines of Dy^{3+} within $4f^9$ configuration (Fig. 5(b)). The emission spectra composed of two groups of emissions peaking at 483 and 575 nm, may be assigned to the Dy^{3+}:4*f* transitions of $^4F_{9/2}$-$^6H_{15/2}$ and $^4F_{9/2}$-$^6H_{13/2}$ respectively[5,14]. The excitation spectra monitoring the 575 and 576 nm emissions consist of a series of lines in the 250–350 nm range with the strongest one at 350 and 326 nm. Also, it can be clearly seen that Ce_2O_3 co-doping increases the luminescence intensity of the Dy^{3+}-doped host lattice, and requires to be investigated in detail.

The after glow process in the $Ca_xMgSi_2O_{5+x}:Dy^{3+}$ (*x*: 1, 2, 3) system has been described earlier by Chen *et al*.[5] According to this study, after irradiation with the ultraviolet light, most of the excitation energy associated with the excited carriers (electrons or holes) will be transferred via the host directly to the luminescence centers, Dy^{3+}, followed by the Dy^{3+} 4*f* emissions as the immediate luminescence. However, part of the excitation energy will be stored when some of the excited carriers drop into the traps, instead of returning to the ground state. Later, with thermal excitation at proper temperature, these carriers will be released from the traps and transferred via the host to the Dy^{3+} ions, followed by the characteristic and persistent Dy^{3+} emissions. In practise, the electron traps and the hole traps may not be both equally abundant or important in terms of their contribution to the long afterglow emission[5].

The excitation spectra (λ_{exc}: 341 nm and 347 nm) of Ce^{3+}-doped $Ca_2MgSi_2O_7$ host, calcined in open and weak reducing atmosphere has been observed as one broad band centered at 395 and 398 nm, respectively (Fig. 6).

The notable point is that main excitation and emission wavelengths are similar for synthesis in

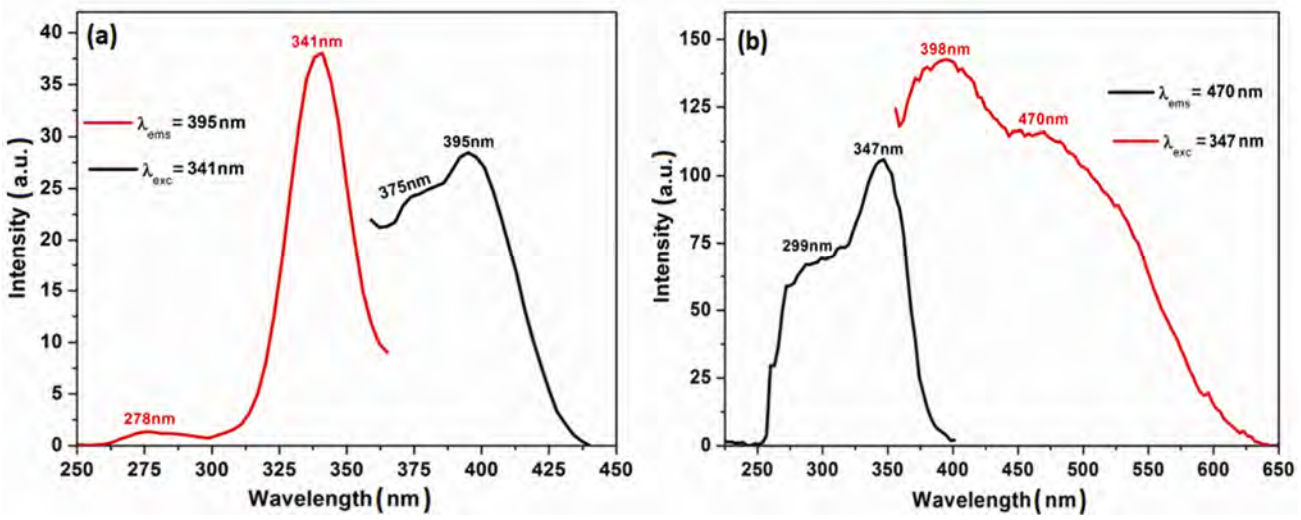

Fig. 6—Excitation and emission spectra of $Ca_2MgSi_2O_7$:0.006Ce^{3+} synthesized in (a) open atmosphere and (b) weak reducing atmosphere.

both open and weak reducing atmospheres, but the Ce-activated phosphor synthesized in weak reducing atmosphere shows a broad blue asymmetric emission band at higher intensity, in addition to white light emission under UV-A excitation.

The asymmetric band could be excited by the spin orbit coupled into two levels of ground state. The asymmetry peak can be deconvolved into two Gaussian profiles centering at ~390 and ~430 nm, which may be assigned to the transition from the lowest 5*d* level to $^2F_{5/2}$ and $^2F_{7/2}$, respectively. The energy difference between the spin-orbit splitting of the 4*f* ground state ($\Delta E = 1/\lambda_1 - 1/\lambda_2$) in $Ca_2MgSi_2O_7$:Ce^{3+} is about 2254 cm^{-1}, which agrees with the theoretical value (2000 cm^{-1})[17]. Ce^{3+} doping in some hosts results in emission spectra near the ultraviolet region. The luminescent colours or wavelengths of these ions change widely from near UV to red region depending on the nature of the host lattices. Alkaline earth silicates, such as Ce^{3+} activated $Ca_3MgSi_2O_8$ phosphor, gave rise to an efficient purple-blue emission under UV excitation and generated two kinds of emission centers in the host[14]. Also, the long lasting phosphorescence was observed in Ce^{3+} doped $Ca_2Al_2SiO_7$ at room temperature[18]. Ce^{3+} ion in åkermanite calcined in reducing atmosphere, which is in the $4f^1$ configuration, showed efficient white luminescence owing to the 4*f*–5*d* transition. The 4*f*–5*d* transition of Ce^{3+} ions in solids is the parity allowed electric dipole transition having large oscillator strengths; such transitions produce efficient broad band luminescence. It has a larger Stokes shift than that of other rare earth ions due to the extended radial wave functions of the 5*d* state. Because of the favourable spectroscopic properties of Ce^{3+} and the ability to incorporate Ce^{3+} into different host materials, cerium activated materials have received renewed interest[18].

Generally, lanthanides exhibit the 3+ oxidation state, since they lose two 6*s* electron and one 5*d*(4*f*) electron to attain the lowest ionization energy. However, due to the presence of either half filled or completely filled or empty 4*f* sub shell, Ce, Pr, Nd, Tb, and Dy can also present the 4+ oxidation state, i.e. Ce^{4+} ($4f^0$), Pr^{4+} ($4f^1$), Nd^{4+} ($4f^2$), Tb^{4+} ($4f^7$), and Dy^{4+} ($4f^8$)[19]. Praseodymium oxides have attracted in the recent years because of their optical, electronic, and chemical properties. The PrO_x system has a similar series having the general formula, Pr_nO_{2n-2} with n= 4, 5, 6, 7, 9, 10, 11, 12, ∞. The Pr^{3+} oxide phase, i.e., Pr_2O_3, has also a hexagonal structure. This structure is characteristic for stoichiometric Pr^{4+} oxide (α-PrO_2). The phases intermediate between Pr^{3+} and Pr^{4+} oxides (β-Pr_6O_{11}, δ-$Pr_{11}O_{20}$, ε-Pr_5O_9, ξ -Pr_9O_{16}, ι-Pr_7O_{12}, Pr_6O_{10} and Pr_5O_8) are classified into the oxygen-deficient modifications of the fluorite structure. Since the most stable phase of the neighboring rare earth oxide (REO) praseodymia is Pr_6O_{11}, exhibiting a mixed valence state (Pr^{4+}/Pr^{3+}) and the highest oxygen exchange activity among all rare earth oxides at atmospheric pressure and room temperature[20], Pr_6O_{11} has been used as the source of Pr^{3+} or Pr^{4+}-ions in the present study.

The excitation and emission spectra of Pr_6O_{11}-doped $Ca_2MgSi_2O_7$ phosphor which is calcined under open atmosphere is presented in Fig. 7(a). There are

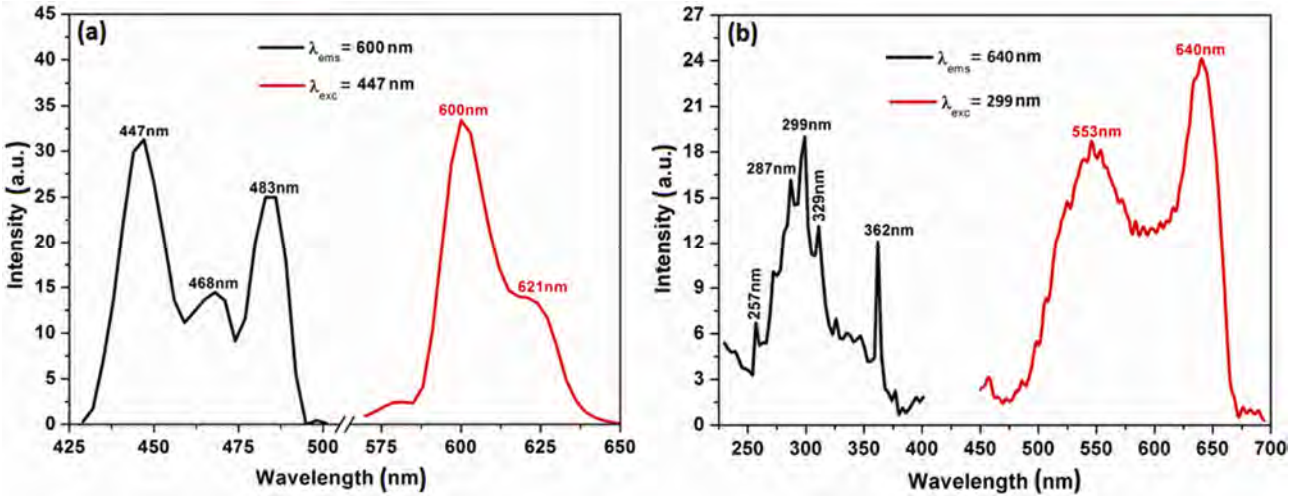

Fig. 7—Excitation and emission spectra of $Ca_2MgSi_2O_7$:0.006Pr^{3+}/Pr^{4+} synthesized in (a) open atmosphere and (b) weak reducing atmosphere.

three excitation peaks at 447 nm ($^3H_4$-$^3P_2$), 468 nm ($^3H_4$-$^3P_1$) and 483 nm ($^3H_4$-$^3P_0$) and the strongest peak is at 447 nm. Significantly, the sharp emission peak at 600 nm and the half peak which is joined to the main peak can be seen in Fig. 7 (b). The main emission peak corresponds to $^1D_2$-$^3H_4$ transition of Pr^{3+}. In the $Ca_2MgSi_2O_7$ crystal lattice, the praseodymium ions are substituted for the Ca^{2+} ions, both as trivalent (Pr^{3+}) and tetravalent (Pr^{4+}) states and the red color is exclusively caused by the Pr^{4+} ions since the calcination atmosphere is appropriate to maintain Pr^{4+} ions in Pr_6O_{11}.

Pr_6O_{11}-added, or more clearly Pr^{3+}-doped phosphors with full color luminescence have received substantial interest because the Pr^{3+} ions exhibit different emissions according to the host lattice in which they are incorporated, e.g., red (from the $^1D_2$ level), green (from the $^3P_0$ level), blue (from the $^1S_0$ level) and ultraviolet (from the 4*f*–5*d* state)[21]. The phosphorescence of 640 nm (red) and 553 nm (green) emission in the sample synthesized in weak reducing atmosphere is derived from $^3P_0 \rightarrow {}^3H_6$ and $^3P_0 \rightarrow {}^3H_5$ transitions of Pr^{3+} under 299 nm UV excitation (Fig. 7(b)).

Pr_6O_{11} (i.e. Pr^{3+}/Pr^{4+}) source for the present study is composed of Pr_2O_3 and PrO_2, and the Pr_6O_{11} doping process of can be defined by Eqs (1-3).

$$PrO_2 \xrightarrow{Ca_2MgSi_2O_7} Pr^{\bullet\bullet}_{Ca} + V''_{Ca} + O_2 \uparrow \quad \ldots (1)$$

$$PrO_3 \xrightarrow{Ca_2MgSi_2O_7} 2Pr^{\bullet}_{Ca} + V''_{Ca} + \frac{3}{2}O_2 \uparrow \quad \ldots (2)$$

$$PrO_3 \xrightarrow{Ca_2MgSi_2O_7} 2Pr^{\bullet}_{Ca} + 2e' + V''_{Ca} + \frac{3}{2}O_2 \uparrow \quad \ldots (3)$$

$Pr^{\bullet\bullet}_{Ca}$ represents vacancy with two positive charge when Pr^{4+} ion takes up the Ca^{2+} site. $Pr^{\bullet}_{Ca}$ represents a vacancy with a positive charge when Pr^{3+} ion takes up a Ca^{2+} site. V''_{Ca} is the vacant site of a Ca^{2+} site and e' is a quasi-free electron.

Previous works have shown that RE^{3+} ions are randomly distributed over the same cationic sites of Ca^{2+} in the $Ca_2MgSi_2O_7$ host[6]. According to Kröger-Vink notation, Pr^{4+} occupies the position of Ca^{2+} on PrO_2 doping. Cation vacancy is generated to compensate charge for the non-equivalence susbstitution as in Eq. (1). When Pr_2O_3 is added to the host, the Pr^{3+} ions occupy the Ca^{2+} sites with the cation vacancies created to compensate charge as seen in Eq. (2). The $Pr^{\bullet}_{Ca}$ vacancy may also be compensated by the quasi-free electron, which is generated from the 5*d* band of Pr^{3+} (Eq. (3))[18]. The presence of Pr in $Ca_2MgSi_2O_7$ requires to be be investigated in detail by X-ray absorption nearedge spectroscopy (XANES) to determine valences of both 3+ and 4+ or one of them.

The rare earth Sm^{3+} with a $4f^5$ electron configuration is often regarded as an efficient activator or co-activator to enhance luminescence intensity. It has complex energy levels and various possible transitions between *f* levels exhibit a strong orange-red fluorescence. The transitions obtained between these *f* levels are highly marked and the spectral lines are sharp[23].

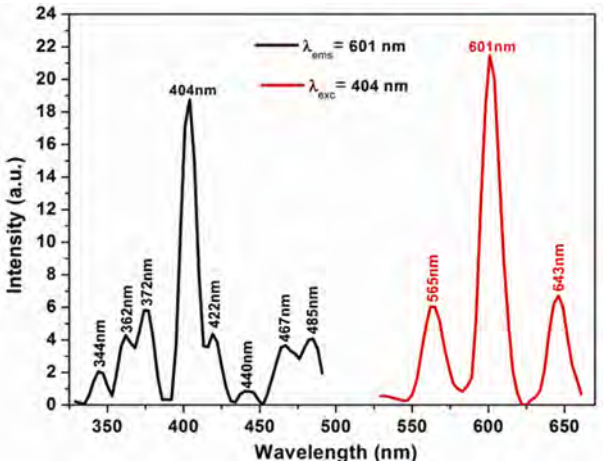

Fig. 8—Excitation and emission spectra of $Ca_2MgSi_2O_7$:0.006Sm^{3+} synthesized in open atmosphere.

The excitation and emission spectra of Sm_2O_3 added as Sm^{3+} source for $Ca_2MgSi_2O_7$ host synthesized in open atmosphere is shown in Fig. 8. The excitation spectra of Sm^{3+}-doped phosphor shows eight excitation bands, i.e., $^6H_{5/2} \rightarrow {}^3H_{7/2}$, $^6H_{5/2} \rightarrow {}^4F_{9/2}$, $^6H_{5/2} \rightarrow {}^4K_{13/2}$, $^6H_{5/2} \rightarrow {}^4F_{7/2}$, $^6H_{5/2} \rightarrow ({}^6P_{5/2}, {}^4P_{5/2})$, $^6H_{5/2} \rightarrow {}^4G_{9/2}$, $^6H_{5/2} \rightarrow {}^4F_{5/2}+{}^4I_{13/2}$, $^6H_{5/2} \rightarrow {}^4I_{9/2}$ transitions at 344, 362, 372, 404, 422, 440, 467 and 485 nm respectively. The emission transitions of the same sample are positioned at 565 nm ($^4G_{5/2} \rightarrow {}^6H_{5/2}$), 601 nm ($^4G_{5/2} \rightarrow {}^6H_{7/2}$) and 643 nm ($^4G_{5/2} \rightarrow {}^6H_{9/2}$), respectively[15,24,25]. The major orange color region emission among three emission transitions is due to the $^4G_{5/2} \rightarrow {}^6H_{7/2}$ transition at 601 nm.

Conclusions

Novel phosphors, $Eu^{2+/3+}$, Dy^{3+}, Ce^{3+}, $Pr^{3+/4+}$, Sm^{3+} separately-doped single-phased $Ca_2MgSi_2O_7$ were synthesized by conventional solid-state reaction method under open (air) atmosphere and/or weak reducing atmosphere comprising nitrogen and hydrogen and its luminescence properties have been investigated. The $Ca_2MgSi_2O_7$ host structure exhibited emission of different colors due to the transitions of each doped rare earth ions. The difference in the measured emission spectra is either due to different emission centers or same emission center with different ionic states occupying in the same host lattice. The results show that Ce^{3+}-doping generated visible white light emission from the åkermanite type phosphor. The study shows that the rare earth ions ($REI^{3+/4+}$) change the emission properties of the samples.

Acknowledgement

The authors thank the Small and Medium Enterprises Development Organization Projects (KOSGEB), 2011/7, Republic of Turkiye, for the financial support.

References

1 Birkel A, Darago L E, Morrison A, Lory A, George N C, Mikhailovsky A A, Birkel C S & Seshadri R, *Solid State Sci*, 14 (2012) 739.
2 Jiang L, Chang C, Mao D & Feng C, *Mater Sci Eng*: B103 (2003) 271.
3 Kyeong Y J, Kook H H, Kang Y C & Ha-Kyun J, *Mater Chem Phy*, 98 (2006) 330.
4 Yi T & Dongying J, *Adv Mater Sci Tech*, 675-677 (2011) 1089.
5 Chen Y, Cheng X, Liu M, Qi Z & Shi C, *J Lumin*, 129 (2009) 531.
6 Lin L, Zhonghua Z, Weiping Z, Zhiqiang Z & Min Y, *J R Earths*, 27(5) (2009) 749.
7 Dhaouadi H, Chaabane H & Touati F, *Nano-Micro Lett*, 3 (3) (2011) 153.
8 Murakami F S, Rodrigues P O, Teixeira de Campos C M & Silva M A S, *Ciênc Tecnol Aliment*, 27 (2007) 3.
9 El Kazazz H, Karacaoglu E, Karasu B & Agatekin M, *J Am Sci*, 7 (2012) 12.
10 Kaya Y S, Karacaoglu E & Karasu B, *Ceramic Int*, 38 (2012) 3701.
11 Kaya Y S, Karacaoglu E & Karasu B, *Adv Appl Ceramic: Struct Funct Bio*, 111 (2012).
12 Karacaoglu E & Karasu B, *Mater Res Bull*, 48 (2013) 3702.
13 Hölsä J, Kirm M, Laamanen T, Lastusaari M, Niittykoski J & Raud J, http://hasyweb.desy.de, *Annual Reports 2006; Part 1*.
14 Jiang L, Chang C & Mao D, *J Al Comp*, 360 (2003) 193.
15 Öztürk E & Karacaoglu E, *J Therm Anal Cal*, 119 (2015) 1063.
16 Su Q, Liang H, Li C, He H, Lu Y, Li J & Tao Y, *J Lumin*, 122 (123) (2007) 927.
17 Gong Y, Wang Y, Xu X, Li Y & Jiang Z, *J Electrochem Soc*, 156 (10) (2009) 295.
18 Bhatkar V B, Omanwar S K & Moharil S V, *Op Mater*, 29 (2007) 1066.
19 Zhu F, Xiao Z, Yan L, Zhang F & Huang A, *Appl Phys A*, 101 (2010) 689.
20 Wang X, Yang C, Wang T M & Liu P, *Electrochim Acta*, 58 (2011) 193.
21 Shih H-R, Tsai Y-Y, Liu K-T, Liao Y-Z & Chang Y-S, *Opt Mater*, 35(12) (2013) 2654.
22 Yan X, *PhD Thesis*, (*Wolfson Centre for Materials Processing Brunel Univ*), 2012.
23 Han B, Zhang J, Li P & Shi H, *Mater Lett*, 126 (2014) 113.
24 Rudramadevi B H & Buddhudu D, *Indian J Pure Appl Phy*, 46 (2008) 825.
25 Li Y-C, Chang Y-H, Lin Y-F, Chang Y-S & Lin Y-J, *J Alloys Comp*, 439 (2007) 367.